Research paper

Experimental investigation of surface crack density and recast layer thickness of WEDMed Inconel 825

P. Kumar[a,b*], M. Gupta[b] and V. Kumar[c]

[a]*Department of Mechanical Engineering, Chandigarh Engineering College, Landran ,Mohali, India*
[b]*Department of Mechanical Engineering, National Institute of Technology, Kurukshetra, India*
[c]*Department of Mechanical Engineering, UIET, Maharishi Dayanand University, Rohtak, India*

Abstract

The present research attempts to analyze the surface topography of WEDMed Inconel 825 concerning surface crack density (SCD_i) and recast layer thickness (RCL_t). Formation of cracks, recast layer, and heat-affected zone are the major issues in determining the final performance of the WEDM machined sample. In this study, WEDM characteristics *viz.* pulse on time (T_{on}), pulse off time (T_{off}), gap voltage (SV), peak current (IP), wire tension (WT), and wire feed (WF) are optimized for the response SCD_i and RCL_t by response surface methodology. The outcome manifests that the topography of the machined surface becomes more rougher at the increased value of T_{on}, IP, and SV. RSM emerges as a great tool in the development of a predicted model based on the desirability approach and finding optimal parametric combinationm which results in reduced SCD_i and RCL_t. At the optimum combination of process parameters, i.e., 109 machine unit T_{on}, 36 machine unit T_{off}, 54 V SV, 120A IP, 9 machine unit WT and 7 m/min WF, the values obtained for SCD_i and RCL_t are 0.00160 $\mu m/\mu m^2$ and 20.991μm, respectively with an error of less than 5%.

1. Introduction

In the engineering field, to meet the diverse demand in quality standards and productivity improvement, superalloys are used as complex materials due to their high-temperature corrosion resistance, oxidation resistance, and creep resistance properties. In the aerospace industry, nickel-based superalloys have widespread use in the manufacturing of combustor casing and engine components [1]. Inconel 825 has been specially developed for aircraft applications because of its high corrosion and high-temperature resistance properties. The surface stability of nickel is readily improved by alloying with chromium and/or aluminum [2]. The properties of Inconel 825, such as high hardness, presence of high abrasive carbide particles, the tendency to weld the cutting tool, and improvement of developed edges, lead it hard to machine with conventional method [3]. WEDM is a vital functioning in several

manufacturing processes where precision and accuracy are of great importance. WEDM has the ability to produce intricate shapes and has a number of key advantages as compared to traditional methods for corrosion resistance and wear resistant electrical conductive materials [4].

Since the WEDM process happens at extremely high temperatures (8000-12000°C), it has a considerable effect on the surface area integrity of the workpiece. The development of high temperature affected zone, microcracks, recast layer, porosity, etc., remains a big problem in the surface structure of machined specimen during the WEDM process [5]. Due to spark erosion, the debris produced by flushing is continuously fed through upper and lower nozzles to the sparking area. The substance which can't be eliminated by dielectric flush re-solidifies, creating a recast layer. This technique additionally prompts pressure bringing about the development of fractures, therefore harming the surface integrity [6]. Surface parameters including micro-hardness, microstructure, residual stress, surface roughness, and surface morphology are really indispensable in deciding the final execution of machined specimens. Surface integrity associated with the sample is emphatically associated with the surface equality of the work material, and in this way adds to its physical properties. Therefore, to decrease surface roughness, the analysis of outcome of WEDM machining parameters on surface crack density (SCD_i) and recast layer thickness (RCL_t) is very important [7-11].

It is apparent from the published studies that discharge power is regarded as the most affecting parameter. Puri and Bhattacharyya [12] analyzed the white layer depth developed in the WEDM process through RSM. An increase in pulse-on time brought about increased white layer depth (WLD) during the very first cut, while a sharp reduction in WLD was observed with increment in T_{on} during trim cutting. Goswami et al. [13] observed that the samples machined with the WEDM display harsher surface region with bunches of developed edge layers at high energy input rate, and more noteworthy surface quality was received under low power input conditions. Li et al. [14]

observed prevailing coral reef-like microstructures at high discharge energy, while arbitrary small-scale voids are predominant at low discharge energy in the machining of Inconel 718. Aspinwall et al. [15] reported that during machining of Inconel 718 with the WEDM, workpiece surface damage is extremely low at high frequency/short pulses duration. Microstructural profile data, like average recast thickness, were observed to be less than 11 µm which means there is no surface damage. Thakur et al. [16] investigated that during dried-up machining of Inconel 825, the surface integrity of machined specimen is affected by cutting speed and multilayer covering substance vapor deposition (CVD). It was noticed that white layer thickness increases with expansion in the cutting speed and decreases at the low value of cutting velocity with CVD coated cemented carbide. Surface integrity analysis of machined specimens also includes tiny craters, microcracks, pockmarks, and recast layer. Crater diameter and crater depth on tool and workpiece surface are very important parameters to study. Tosun et al. [17] found that crater diameter and crater depth increase with expansion in amenable circuit voltage, pulse duration, and wire speed, whereas dielectric flushing stress is much less successful for deciding the crater diameter and level.

Although many experts have analyzed the surface area integrity belonging to the machined samples, there are not many studies wherein surface integrity has been studied with respect to SCD_i, RCL_t, as well as machining details, ,which has been enhanced to decrease the surface roughness [6, 18]. Although Inconel 825 possesses superior mechanical properties over other nickel-based superalloys, there are no enough investigations to study area integrity qualities of this alloy during WEDM processes. Therefore, this analysis mostly focuses on the impact as well as optimization of machining parameters on SCD_i and RCL_t using WEDM.

2. Materials and methods

2.1. Specimen and equipment

Inconel 825 (150 mm x 150 mm x 10 mm) was put to use as the work material, and brass wire

(0.25 mm) was utilized as the tool electrode. The physical and chemical properties of work material were given in Table 1. Experiments were conducted using sprint cut computer numerical controlled (CNC) wire-cut electrical discharge machine (WEDM), at the Department of Mechanical Engineering, National Institute of Technology, Kurukshetra, Haryana, India, as shown in Fig. 1.

2.2. Experimentation

Reaction surface methodology is really a scientific and factual procedure used to construct, upgrade, and streamline different procedure parameters. RSM gets a relapse model which perceives the communication between the info factors and yield reactions [19]. It can help to find most likely the closest combination of machining parameters past or maybe inside the scope of measure of factors. Based on the outcomes received from the fundamental examinations as well as literature review, six parameters, i.e., pulse on time (T_{on}), pulse off time (T_{off}), peak current (IP), gap voltage (SV), wire tension (WT), and wire feed (WF) were chosen as the input parameters. The microstructural response characteristics were assessed with regards to RCL_t and SCD_i.

2.3. Measurements of surface characteristics

All measurements related to area micrograph were carried out using a scanning electron microscope (JEOL, Model 6100, USA); a profile computing microscope, which determines the surface area microstructures, development of recast layer, and heat-affected zone of work substance machined with WEDM.
 Etching was performed using Kroll's reagent (2% (v/v) hydrofluoric acid, 10% (v/v) nitric acid). Next, the samples were cleaned utilizing acetone $(CH_3)_2CO$ and observed under SEM. RCL_t and SCD_i were made by importing the SEM micrograph into Axio-vision software. Cracks on the surface were assessed by acquiring the length of the cracks on each specimen.
Surface crack density and recast layer thickness can be estimated by using the following formulae:

$$SCD_i = LC_i / A_i \qquad (1)[18]$$
where,
SCD_i = Surface crack density;
LC_i = Cracklength (μm);
A_i = Micrographarea (μm^2)

$$RCL_t = RCLA_i / RCL_i \qquad (2)[18]$$
where,
RCL_t = Thickness of Recast layer (μm);
$RCLA_i$ = Area of Recast layer (μm^2);
RCL_i = Length of Recast layer (μm)

2.4. Design of experiment

Central composite design (CCD) at α value of ± 2 was used using Design Expert software (version 9.0.7, Statease) to enhance the amounts of significant variables. Table 2 shows the coded and real values of the variables.
A regression equation was created to produce an exact model to relates the responses to the procedure factors of investigation.

$$y = \beta_o + \sum_{i=1}^{k} \beta_i x_i + \sum_{i=1}^{k} \beta_{ii} x_i^2 + \sum_{i<j}^{k} \beta_{ij} x_i x_j \pm \varepsilon \qquad (3)$$

where, Y is definitely the expected result (SCD_i, RCL_t), β_0 is the constant term, β_i is the linear coefficients, β_{ii} is the squared coefficients, and β_{ij} is the interaction coefficients. The nature of fitting by the polynomial model condition was expressed using the coefficient of determination R^2. Eq. (3) was utilized to develop 3D plots.

Fig. 1. Sprint cut CNC WEDM machine tool.

2.5. Desirability approach for multi-response optimization of process variables

Desirability functionality strategy was thoroughly utilized for multiple and single quality characteristics problems. Eq. (4) was used to determine the minimum output response (y) and the desirability index (d).

$$d = \begin{cases} 1 & y < T \\ \left(\frac{U-y}{U-T}\right)^{r} & L \leq y \leq T) \\ 0 & y > U \end{cases} \quad \dots (4)$$

Desirability function (d) assigns selection between 0 and 1. d=0, representing the absolutely ominous value, and d=1 representing the absolutely desirable value. Global desirability (D), the blend of specific desirability for every result, can be estimated using the following equation:

$$D = (d_1 \times d_2 \dots \dots d_m)^{1/m} \quad (5)$$

where, m is the variety of responses.

The optimization procedure searches the maximum value of SCD_i and RCL_t by minimizing the SCD_i and RCL_t. Response data were produced both for individual as well as multiple effects. An answer was created with expected measures of the impartial variables and predicted least SCD_i and minimum RCL_t.

2.6. Validation experiments

To ensure the validity of the selected model, experiments were developed using the expected optimum values of parameters. The responses were calculated and compared with the expected value. Experiments were conducted in triplicates and also the data provided as mean ± SD.

3. Results and discussion

Response surface methodology is an empirical model that correlates the input variables with the output responses. The six parameters, i.e., T_{on}, T_{off}, IP, SV, WT, and and WF were selected as the input parameters; 52 experiments in total were conducted (Table 1).

Table 1. Central composite RSM design with actual responses.

Run	T_{on}	T_{off}	SV	IP	WT	WF	SCD_i	RCL_t
1	0	0	0	0	0	-2.38	0.0058	24.89
2	0	0	0	0	0	0	0.0073	25.03
3	-1	-1	1	1	1	1	0.0087	26.83
4	1	-1	1	-1	1	1	0.0081	25.67
5	1	1	1	-1	-1	1	0.0110	24.43
6	1	-1	1	-1	-1	-1	0.0059	26.56
7	1	1	-1	1	-1	1	0.0130	30.30
8	0	0	0	0	0	0	0.0073	23.89
9	-1	1	-1	-1	-1	1	0.0028	21.96
10	-1	-1	1	1	-1	-1	0.0061	22.99
11	1	1	-1	1	1	-1	0.0068	25.80
12	-1	1	1	1	-1	1	0.0063	22.83
13	-1	1	-1	1	-1	-1	0.0047	22.40
14	1	-1	-1	-1	-1	1	0.0100	28.20
15	0	0	0	0	0	0	0.0082	24.02
16	0	0	0	0	0	0	0.0073	25.87
17	-1	-1	-1	1	-1	1	0.0065	25.61
18	2.38	0	0	0	0	0	0.0138	34.62
19	1	-1	-1	1	1	1	0.0110	28.89
20	0	-2.38	0	0	0	0	0.0085	26.70
21	0	2.38	0	0	0	0	0.0068	24.13
22	1	-1	1	1	1	-1	0.0091	30.85
23	-1	1	1	1	1	-1	0.0068	25.89
24	0	0	0	0	0	0	0.0075	24.13
25	1	1	-1	-1	1	1	0.0078	22.71
26	-1	-1	-1	-1	-1	-1	0.0051	23.56
27	-1	-1	1	-1	1	-1	0.0038	23.67
28	0	0	0	0	-2.38	0	0.0077	25.66
29	0	0	0	2.38	0	0	0.0127	29.27
30	-1	-1	1	-1	-1	1	0.0022	20.47
31	1	1	1	1	1	1	0.0140	31.16
32	0	0	0	0	2.38	0	0.0070	25.17
33	0	0	0	0	0	0	0.0070	24.04
34	-1	-1	-1	1	1	-1	0.0083	22.90
35	0	0	0	0	0	0	0.0072	25.01
36	0	0	-2.38	0	0	0	0.0069	24.59
37	1	1	1	1	-1	-1	0.0130	30.74
38	-1	1	-1	1	1	1	0.0046	23.74
39	-1	1	1	-1	-1	-1	0.0034	20.51
40	1	1	1	-1	1	-1	0.0069	24.93
41	-1	1	1	-1	1	1	0.0051	22.66
42	-1	-1	-1	-1	1	1	0.0053	23.61
43	0	0	2.38	0	0	0	0.0082	26.24
44	1	1	-1	-1	-1	-1	0.0073	26.08
45	1	-1	-1	-1	1	-1	0.0061	23.84
46	-2.38	0	0	0	0	0	0.0014	20.05
47	0	0	0	0	0	2.38	0.0085	25.94
48	1	-1	-1	1	-1	-1	0.0110	31.06
49	1	-1	1	1	-1	1	0.0120	31.08
50	0	0	0	0	0	0	0.0072	25.32
51	-1	1	-1	-1	1	-1	0.0018	20.89
52	0	0	0	-2.38	0	0	0.0023	21.55

Fig. 2. SEM micrograph of the WEDM processed surface at different machining conditions; (a) run 9, (b) run 23, (c) run 30, and (d) run 48.

SEM evaluation was carried out for every 52 runs. The SEM micrographs exhibited the existence of craters, heat-affected zone, pockmarks, pulled-out material, and recast layer (Fig. 2).
Through the SEM micrograph, numbers of cracks, pockmarks, and craters on the material surface can be observed (Fig. 3).
Due to rapid heating and quenching, a multilayered area was created during cutting functioning (Fig. 4). At amazingly top an appearance was seen on work surfacearea perceived as recast layer. because of re-hardening of softened material on the work surface which isn't catapulted by the flushing weight of dielectric liquid. Underneath the recast layer, there is the heat-influenced zone, where no dissolving material is available on the work surface; however, the miniaturized scale structure changes from base material because of an exceptional heat transfer. At the bottom, there is the base material.
Two scientific regression models have been created by RSM for SCD_i and RCL_t, respectively. The accuracy of the models was analyzed by ANOVA for each response. SCD_i and RCL_t values were determined by estimating the length of cracks, zone of recast layer, and area of a micrograph by importing the SEM micrograph of every operation in Axio-vision software (Figs. 3 and 4).

3.1. Analysis of variance for quadratic model of SCD_i

The analysis of variance for the response surface model is summarized in Table 2.

Fig. 3. SCD_i observed at (a) Exp no.18 T_{on} = 115, T_{off} =38, SV = 50, IP=130, WT = 10, WF=6, (b) Exp no.52 T_{on} = 111, T_{off} = 38, SV = 50, IP=107, WT = 10, WF=6, and (C) Exp no. 9 T_{on} = 109, T_{off} =41, SV = 46, IP=120, WT = 9, WF=7.

Fig. 4. Recast layer thickness observed at (a) Exp no.18 T_{on} = 115, T_{off} =38, SV = 50, IP=130, WT = 10, WF=6, (b) Exp no.40 T_{on} = 113, T_{off} = 41, SV = 54, IP=120, WT = 11, WF=5, and (c) Exp no.48 T_{on} = 113, T_{off} =35, SV = 46, IP=140, WT =9, WF=5.

Table 2. Analysis of variance for surface crack density (SCD_i).

Source	Sum of Squares	df	Mean Square	F Value	p-value Prob > F
Model	0.00045	21	2.17E-05	73.64428	< 0.0001
A	0.00023	1	0.000235	798.6885	< 0.0001
B	1.42E-06	1	1.42E-06	4.826799	0.0359
C	4.08E-06	1	4.08E-06	13.86238	0.0008
D	0.00013	1	0.000126	428.911	< 0.0001
E	1.43E-06	1	1.43E-06	4.853403	0.0354
F	1.92E-05	1	1.92E-05	65.17797	< 0.0001
AB	9.03E-06	1	9.03E-06	30.69264	< 0.0001
AC	4.51E-07	1	4.51E-07	1.53357	0.2252
AD	6.05E-07	1	6.05E-07	2.056089	0.1619
AE	1.33E-05	1	1.33E-05	45.06827	< 0.0001
AF	1.15E-05	1	1.15E-05	39.15065	< 0.0001
BC	1.95E-05	1	1.95E-05	66.37683	< 0.0001
BD	3.2E-07	1	3.2E-07	1.087518	0.3054
BE	2.76E-06	1	2.76E-06	9.38409	0.0046
BF	9.8E-07	1	9.8E-07	3.330524	0.0780
CD	3.13E-06	1	3.13E-06	10.62029	0.0028
CE	4.06E-06	1	4.06E-06	13.80213	0.0008
CF	1.8E-07	1	1.8E-07	0.611729	0.4403
DE	5E-09	1	5E-09	0.016992	0.8972
DF	1.01E-07	1	1.01E-07	0.344097	0.5619
EF	1.81E-06	1	1.81E-06	6.134281	0.0191
Residual	8.83E-06	30	2.94E-07		
Lack of Fit	7.91E-06	23	3.44E-07	2.631841	0.0954
Pure Error	9.15E-07	7	1.31E-07		
Cor Total	0.000464	51			
Std. Dev.	0.000542		R^2	0.980971	
Mean	0.007369		Adj R^2	0.96765	
C.V. %	7.360963		Pred R^2	0.930766	
PRESS	3.21E-05		Adeq Precision	35.90169	

The Model p-value of <0.0001 implies that the model is statistically significant. A multiple regression equation was built to explain the correlation between SCD_i and the six process parameters as follows:

SCD_i = +7.369e − 003 + 2.329 e - 003A-1.811 e - 004 B + 3.069 e -004 C + 1.707 e - 003D-1.816 e - 004 E + 6.654 e - 004 F + 5.313 e - 004 AB + 1.188 e -004 AC + 1.375 e - 004 AD-6.437 e -

004 AE + 6.000 e -004 AF + 7.813 e – 004 BC - 1.000 e - 004 BD - 2.937 e - 004 BE + 1.750 e – 004 BF + 3.125 e - 004 CD+3.563 e -004 * C * E+7.500 e -005 * C * F-1.250 e -005 * D * E-5.625 e -005 * D * F+2.375 e -004 * E * F

$$(6)$$

where, A, B, C, D, E, and F are the coded values of T_{on}, T_{off}, SV, IP, WT, and WF, respectively. The p-values <0.05 proposes that the direct (A, B, C, D, E, F) and interactive (AB, AE, AF, BC, BE, CD, CE, EF) model terms have an entirely significant effect on SCD_i. The test for lack of fit was found to be not significant. The p-value for lack of fit is 0.0954, showing that this model fits enough into the information. To guarantee the decency of the model, estimations of predicted R^2 and adjusted R^2 were determined. It ought to be near 1, showing that the observed and predicted values are extremely correlated to one another.The predicted R^2 of 0.9308 is in sensible concurrence with the adjusted R^2 of 0.9677.

3.1.1. Parametric analysis on SCD_i

The impact of individual process parameters on SCD_i is determined by perturbation graph (Fig. 5).
From the steep curve of T_{on}, IP, WF, and SV, it is noticed that SCD_i is highly affected by T_{on} (A) and IP (D).
Three-dimensional plots between T_{on} and T_{off} (AB), T_{on} and IP (AD), T_{off} and IP (BD), T_{off} and SV (BC) with SCD_i are revealed in Fig. 6(a-d), respectively. From Fig. 6(a), it is observed that the value of SCD_i increases significantly from 0.0057 μm/μm^2 to 0.0093 μm/μm^2 with a growth in the importance of pulse-on time from 109 MU to 113 MU. This can be due to the fact that cracks' length and density depend upon the discharge energy.
Discharge energy is actually the function of T_{on}, IP, and SV. As the discharge energy increases, more heat is transferred toward the work surface, which brings about more liquefying and dissipation of work material. Due to intense heat, profound and covering pits were formed on the surface texture of the machined surface [20].

T_{off} has no positive effect on SCD_i, as the increase in value of T_{off} from 35-41 MU, SCD_i decreases from 0.0057 μm/μm^2 to 0.0043 μm/μm2 since the high estimation of T_{off} gives adequate time for deionization in workpiece and tool electrode gap, which in turn decrease the length of microcracks (Fig. 6(a)). Nevertheless, when used in combination, the SCD_i value increases up to 0.010 μm/μm^2, as MRR is highly dependent upon discharge energy. High discharge energy is produced in the discharge gap at high estimation of T_{on}, while low discharge energy is generated as pulse-off time gets increased [21].
Similarly, a significant effect of IP on SCD_i is observed from Fig. 6(b)). SCD_i increases from 0.00347 μm/μm^2 to 0.0066 μm/μm^2 when peak current increases from 120 A to 140 A (Fig. 6(b)). It is evident from the literature that at a high value of peak current, successive electrical discharge builds up and intense heat gets generated, which melts far more content from the surface area resulting in deep craters [22].
From Fig. 6(c), it is noticed that the interactive effect of T_{on} and IP increases the SCD_i up to 0.0114 μm/μm^2. From Fig 6(c), it is noticed that SCD_i is raised from 0.0057 μm/μm^2 to 0.0087 μm/μm^2 with the interaction between T_{off} and IP. An increase in gap voltage from 48 V to 54 V results in a decrease in surface crack density from 0.0079 μm/μm^2 to 0.0071 μm/μm^2 (Fig. 6(d)).
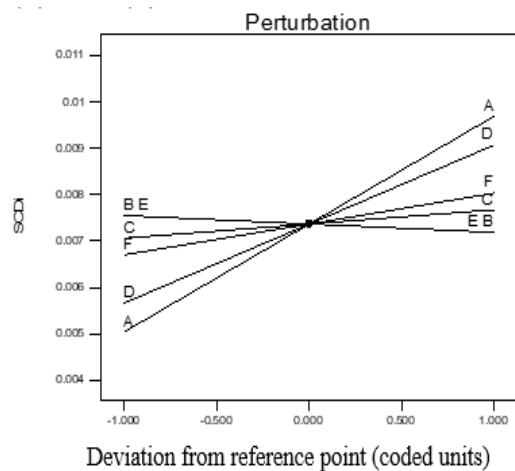
Fig. 5. Perturbation plot showing the effect of individual parameters on surface crack density.

(a)

(b)

(c)

(d)
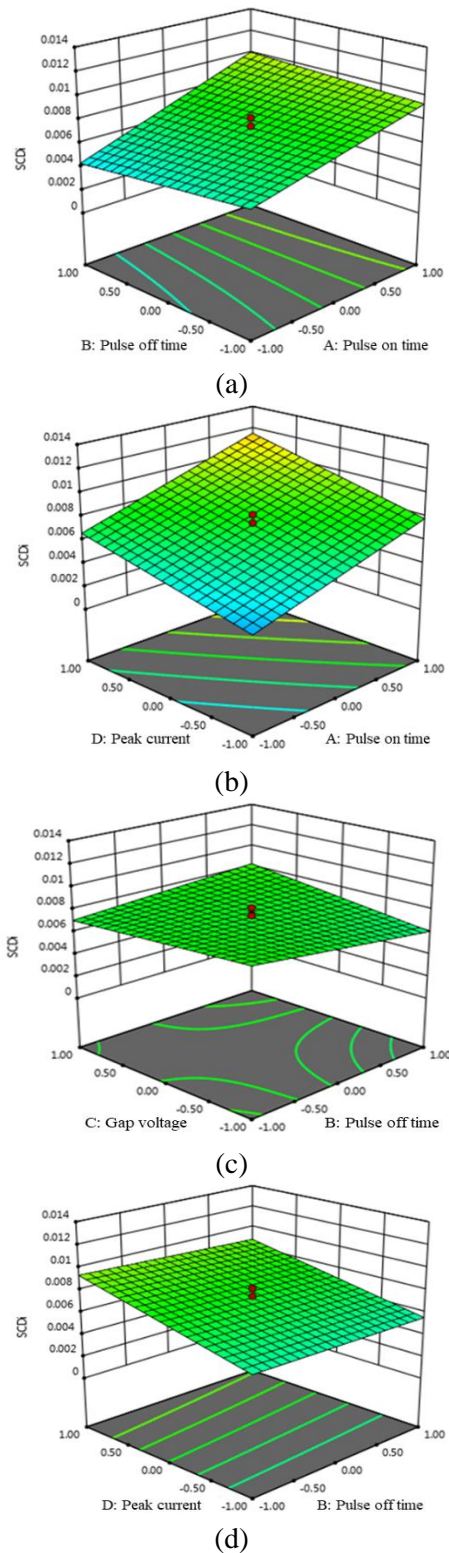
Fig. 6. Three-dimensional plots showing the interaction of (a) $T_{on} \times T_{off}$; (b) $T_{on} \times IP$; (c) $T_{off} \times IP$; (d) $T_{off} \times SV$ on SCD_i when other factors were kept constant.

Table 3. Analysis of variance for RCL_t.

Source	Sum of Squares	Df	Mean Square	F Value	p-value Prob > F
Model	430.284	21	20.489	80.477	< 0.0001
A	220.51	1	220.512	866.094	< 0.0001
B	12.731	1	12.731	50.002	< 0.0001
C	5.218	1	5.218	20.496	< 0.0001
D	114.07	1	114.071	448.03	< 0.0001
E	0.470	1	0.470	1.848	0.1840
F	2.104	1	2.104	8.265	0.0074
AB	0.000	1	0.0007	0.002	0.9584
AC	2.392	1	2.392	9.397	0.0046
AD	12.763	1	12.763	50.131	< 0.0001
AE	16.632	1	16.632	65.324	< 0.0001
AF	0.236	1	0.236	0.928	0.3430
BC	2.673	1	2.673	10.501	0.0029
BD	0.411	1	0.411	1.617	0.2132
BE	0.155	1	0.155	0.610	0.4408
BF	0.444	1	0.444	1.744	0.1966
CD	5.436	1	5.436	21.353	< 0.0001
CE	26.772	1	26.772	105.154	< 0.0001
CF	3.706	1	3.706	14.555	0.0006
DE	0.181	1	0.181	0.712	0.4052
DF	2.838	1	2.838	11.147	0.0023
EF	0.533	1	0.533	2.0935	0.1583
Residual	7.638	30	0.254		
Lack of Fit	3.811	23	0.165	0.303	0.9860
Pure Error	3.826	7	0.546		
Cor Total	437.92	51			
Std. Dev.	0.504		R^2	0.982	
Mean	25.298		Adj R^2	0.970	
C.V. %	1.994		Pred R^2	0.975	
PRESS	10.608		Adeq Precision	33.859	

The results can be manifested to a high value of SV (54 V), leading to an increased gap between tool and workpiece, which causes reduced machining rate and numbers of electric sparks [23]. At a low value of SV (46 V), the gap between tool and workpiece becomes narrow and the number of electric spark increases causing ts machining rate to increase [23]. The parameters like WF and WT have a less positive effect on SCD_i and RCL_t.

3.2. Analysis of variance for RCL_t

ANOVA for the response surface model of recast layer thickness is provided in Table 3.
The Model F-estimation of 80.48 implies that the unit is actually significant with just a 0.01% probability that a "Model F-value" of this enormous value might happen due to noise. Based on test results, a prescient two-factor polynomial condition was worked to clarify the connection among's RCL_t and the six process parameters as follows:

$$RCL_t = +25.30 +2.26\ A -0.54\ B + 0.35\ C + 1.62\ D - 0.10\ E + 0.22\ F +4.688E\text{-}003\ AB +0.27\ AC +0.63\ AD -0.72\ AE -0.086\ AF +0.29\ BC +0.11\ BD +0.070\ BE -0.12\ BF + 0.41\ CD +0.91\ CE - 0.34\ CF +0.075\ DE +0.30\ DF +0.13\ EF$$

(7)

Estimations of "Prob > F" under 0.0500 shows that the model is really significant. In this case, A, B, C, D, F, AC, AD, AE, BC, CD, CE, CF, and DF are actually effective model terms. The "Lack of Fit" F-value of 0.30 shows that lack of fit is not significantly distant relative to the pure error. There is a 98.60% chance that the lack of fit F-value of this large might happen due to noise. The "Pred R-Squared" of 0.9758 is actually in practical agreement with the "Adj R-Squared" of 0.9703. "Adeq Precision" measures the signal-to-noise ratio. The ratio of 33.859 indicates an adequate signal.

3.2.1. Parametric analysis on RCL_t

From the Perturbation graph, it is noticed that T_{on} and IP have a significant effect on Fig. 7.
The three-dimensional plot between T_{on} and T_{off} (AB), T_{on} and IP (AD), T_{off} and IP (BD), and T_{off} and SV (BC) with SCD_i are shown in Fig. 8(a-d), respectively.
From Fig. 8(a), it is observed that RCL_t increases from 23.232 μm to 27.676 μm with an increment in T_{on} from 190 μs to 113 μs and decreases from 23.232 μm to 22.136 μm with an increase in pulse off time from 35 Machine unit to 41 Machine unit. T_{on} is an actually prominent factor that increases the RCL_t. As T_{on} increases, the discharge energy increments and flashes focus in the hole builds, which brings about progressively material dissolved from the surface.

Subsequently, the dielectric pressure can't flush the extinguished metal from the surface, and a thicker layer gets saved on a superficial level, known as the recast layer [24].
When applied in combination, the recast layer thickness slightly decreases up to 26.610 μm. From Fig. 8(b), it is observed that peak current is an influencing parameter for recast layer.
With the increase in peak current from 120 A to 140 A, thevrecast layer increases from 21.682 μm to 23.642 μm. At a high value of IP, more material melts resulting in the formation of a thicker recast layer. Only a slight increase in the recast layer thickness (25.38 μm to 25.51 μm) is observed when servo voltage increases from 46 V to 54 V. An increment in the gap voltage stabilizes the electric discharge or decreases the discharge delay time, which results in a slower machining rate and material removal rate [24].

3.3. Multi response optimization using desirability function

Desirability functionality strategy is thoroughly utilized for multiple and single quality characterization problems. The optimization process finds the optimum worth of six parameters by minimizing the SCD_i and RCL_t. Examinations were done under anticipated conditions as given by the program. It is observed that at 109 Machine unit T_{on}, 36 Machine unit T_{off}, 54 V SV, 120 A IP, 9 Machine unit WT, and 7 m/min WF, the values obtained for SCD_i and RCL_t are 0.00160 μm/μm² (Fig. 9(a)) and 20.991 μm (Fig. 9(b)), respectively, with an error of less than 5% (Table 4). Thus, the model is successfully validated. The desirability index of the model is 0.954 (Fig. 10).
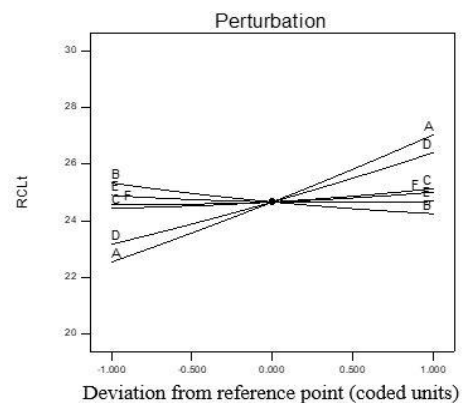
Fig. 7. Perturbation plot showing the effect of individual parameters on thetrecast layer thickness.
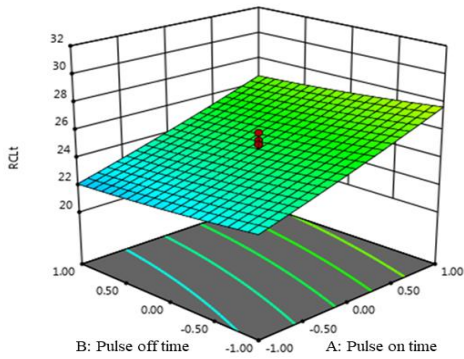
(a)
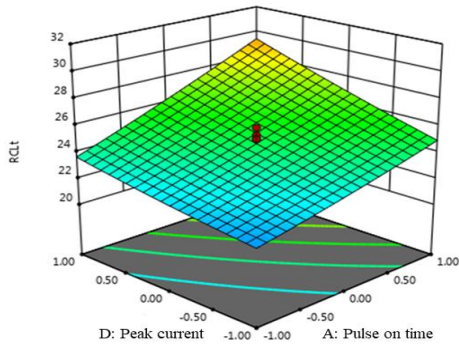
(b)
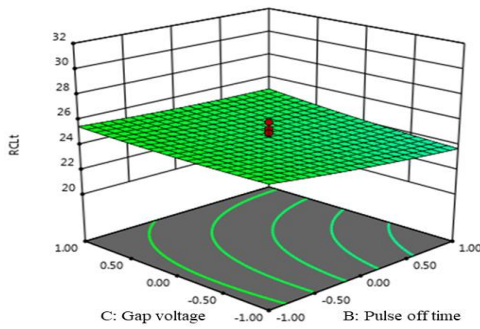
(c)
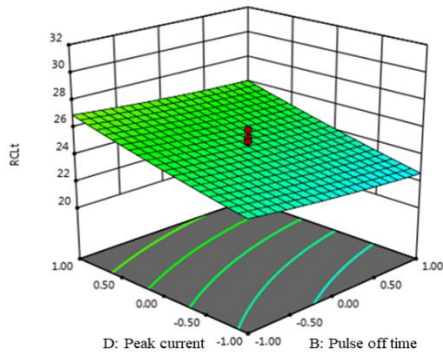
(d)

Fig. 8. 3-D plot showing the interaction of (a) Ton×Toff, (b) Ton× IP, (c) Toff × SV, and (d) $T_{off} \times$ IPon RCL_t when other factors were kept constant.
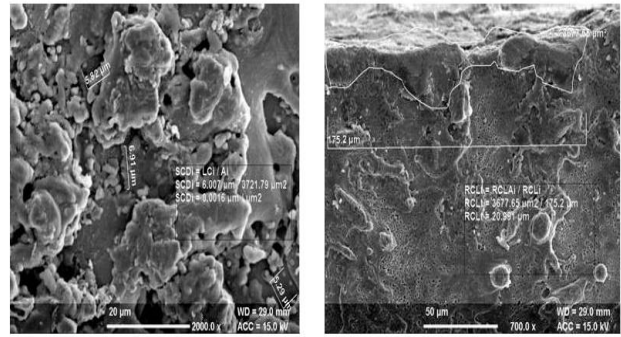
(a)   (b)

Fig. 9. Surface crack density and recast layer thickness observed under optimized run; (a) SCD_i and (b) RCL_t.

Table 4. Validation of predicted model

Objective	Optimization parameters						Predicted values	Confirmatory results
	T_{on}	T_{off}	SV	IP	WT	WF		
SCD_i ($\mu m/\mu m^2$)	109	36	54	120	9	7	0.0020	0.00160
RCL_t (μm)							20.050	20.991
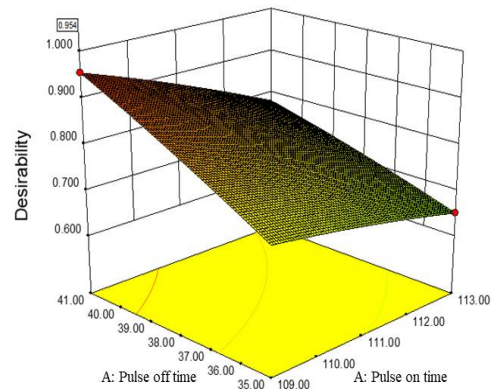
Fig. 10. 3-D graph showing the desirability index of optimized run.

4. Conclusions

The following conclusions are drawn from the present research:

Pulse-on time and peak current fundamentally influence the surface of the machined specimen. At the high value of T_{on} and IP, deep and wider craters, cracks and pockmarks are seen on the machined surface because of the dissolving and vanishing of material from the surface. WF and WT are found less significant for SCD_i

RCL_t is highly affected by pulse-on time. Pulse-off time and gap voltage are seen as less

noteworthy. It is noticed that at the most ideal combination of process parameters, i.e., 109 Machine unit T_{on}, 36 Machine unit T_{off}, 54 V SV, 120 A IP, 9 Machine unit WT, and 7 m/min WF, the values obtained for SCD_i and RCL_t are 0.00160 $\mu m/\mu m^2$ and 20.991 μm, respectively with an error of less than 5%. The desirability index of the model is 0.954.

References

[1] G. R. Thellaputta, S. C. Pulcharu and C. S. P. Rao, "Machinability of Nickel Based Superalloys: A Review", *Mater. Today: Proc.*, Vol. 4, No. 2, pp. 3712-3721, (2017).

[2] P. Kumar, Meenu, V. Kumar, "Optimization of Process Parameters for WEDM of Inconel 825 Using Grey Relational Analysis", Decision *Sci. let.,* Vol. 7, No. 4, pp. 405-416, (2018).

[3] A. Singh, S. Anandita and S. Gangopadhyay, "Microstructural analysis and multi response optimization during ECM of Inconel 825 using hybrid approach", *Mater. Manuf. Process.,* Vol. 30, No. 7, pp. 842-851, (2015).

[4] M. Y. Ali, A. Banu and M. A. Bakar, "Influence of Wire Electrical Discharge Machining (WEDM) process parameters on surface roughness", *Mater. Sci. Eng.*, Vol. 290, No. 1, p. 012019, (2017).

[5] Y. Shen, Y. Liu, H. Dong and K. Zhang, "Surface integrity of Inconel 718 in high-speed electrical discharge machining milling using air dielectric", *Int. J. Adv. Manuf. Technol.,* Vol. 90, No. 1-4, pp. 691-698, (2017).

[6] Z. Zhang, W. Ming and H. Huang, "Optimization of process parameters on surface integrity in wire electrical discharge machining of tungsten tool YG15", *Int. J. Adv. Manuf Technol,* Vol. 81,No. 5-8, pp.1303–1317, (2015).

[7] K. Kanlayasiri and S. Boonmung, "Effects of wire-EDM machining variables on surface roughness of newly developed DC 53 die steel: Design of experiments and regression model", *J. Mater. Process. Technol.,* Vol. 192-193 No. 1, pp. 459-464, (2007).

[8] C. Chuanliang, Z. Xianglin, Z. Xiang and D. Chunfa, "Surface Integrity of Tool Steels Multi-cut by Wire Electrical Discharge Machining", *Procedia Eng.,* Vol. 81, pp.1945-1951, (2014).

[9] N. Z. Khan, Z. A. Khan, A. N. Siddiquee and A. K. Chanda, "Investigations on the effect of wire EDM process parameters on surface integrity of HSLA: a multi-performance characteristics optimization", *Prod. Manuf. Res.*, Vol. 2, No.1, pp. 501–518, (2014).

[10] Z. Chen Z. Moverare, R. L. Peng and S. Johansson, "Surface Integrity and Fatigue Performance of Inconel 718 in Wire electrical discharge machining, *Procedia CIRP,* Vol. 45, pp. 307-310, (2016).

[11] M. P. Garg, A. Kumar and C. K. Sahu, "Mathematical modeling and analysis of WEDM machining parameters of nickel-based super alloy using response surface methodology", *Sadhana* Vol. 42, No. 6, pp. 981–1005, (2017).

[12] A. B. Puri and B. Bhattacharyya, "Modeling and analysis of white layer depth in a wire-cut EDM process through response surface methodology" *Int. J. Adv. Manuf. Technol.,* Vol. 25, No. 3-4, pp. 301–307, (2005).

[13] A. Goswami and J. Kumar, "Trim cut machining and surface integrity analysis of Nimonic 80A alloy using wire cut EDM", *Eng. Sci. Technol., Int. J.*, Vol. 20, No. 1, pp. 175–186, (2017).

[14] L. Li, Y. B. Guo, X. T. Wei and W. Li, "Surface integrity characteristics in wire-EDM of inconel 718 at different discharge energy", *Procedia CIRP*, Vol. 6, pp. 220-225, (2013).

[15] D. K. Aspinwall, S. L. Soo, A. E. Berrisford and G. Walder, "Workpiece surface roughness and integrity after WEDM of Ti6Al4V and Inconel 718 using minimum damage generator technology", *CIRP Annal.,* Vol. 57, No. 1, pp. 187-190, (2008).

[16] A. Thakur, A. Mohanty, S. Gangopadhyay and K. P. Maity, "Tool wear and chip

characteristics during dry turning of Inconel 825" *Procedia Mater. Sci.*, Vol. 5, pp. 2169-2177, (2014).

[17] N. Tosun and H. Pihtili, "The Effect of Cutting Parameters on Wire Crater Sizes in Wire EDM" *Int. J. Adv. Manuf. Technol.,* Vol. 21, No. 10-11, pp. 857-865, (2003).

[18] A. Kumar, V. Kumar and J. Kumar, "Surface crack density and recast layer thickness analysis in WEDM process through response surface methodology" *Mach. Sci. Technol.*, Vol. 20, No. 2, pp. 201-230, (2016).

[19] P. Kumar, M. Gupta, V. Kumar, "Microstructural analysis and multiresponse optimization of WEDM of Inconel825 using RSM based desirability approach" *J. Mech. Behav. Mater.*, Vol. 28, No. 1, pp. 39–61, (2019).

[20] B. Khosrozadeh, M. Shabgard, "Effects of hybrid electrical discharge machining processes on surface integrity and residual stresses of Ti-6Al-4V titanium alloy", *Int J. Adv. Manuf. Technol.,* Vol. 93, No. 5, pp. 1999-2011, (2017).

[21] D. Mishra and S. A. H. Rizvi, "Influence of EDM parameters on MRR, TWR and surface integrity of AISI 4340", *Int. J. Tech. Res. Appl.*, Vol. 42, pp. 95-98, (2017).

[22] P. Kumar, M. Gupta and V. Kumar, "Experimental analysis of WEDM machined surface of Inconel 825 using single objective PSO" *J. Phys.: Conf. Series*, Vol. 1240, No. 1, p. 012053, pp.1-10, (2019).

[23] P. S. Rao, K. Ramji and B. Satyanarayana, "Effect of wire EDM conditions on generation of residual stresses in machining of aluminum 2014 T6 alloy", *Alexandria Eng. J.*, Vol. 55, No. 2, pp.1077-1084, (2016).

[24] M. Kolli and A. Kumar, "Effect of dielectric fluid with surfactant and graphite powder on Electrical Discharge Machining of titanium alloy using Taguchi method", *Eng. Sci. Technol., Int. J.,* Vol.18, No. 4, pp. 524-535, (2015).

How to cite this paper: